Geometric Solution to Probabilistic Admissible Region (G-PAR)

Utkarsh R. Mishra
Texas A&M University
Suman Chakravorty
Texas A&M University

Islam I. Hussein
Trusted Space

Weston Faber
L3Harris Technologies

Siamak Hesar
Kayhan Space Corporation

Benjamin Sunderland
Kayhan Space Corporation

ABSTRACT

Probabilistic Admissible Region (PAR) is a technique to initialize the probability density function (pdf) of the states of a Resident Space Object (RSO). It combines apriori information about a few of the orbital elements, in the form of postulated statistics, and a single partial-state observation to initialize the pdf of the states of an RSO. A geometrical solution to Probabilistic Admissible Region (PAR) with angles-only telescope observations is presented. The new formulation gives a closed-form solution for PAR particle mapping for the first time. The G-PAR based initialization of the pdf of an object in Medium Earth Orbit (MEO) is shown. Next, a recursive filter that uses successive measurements to update the pdf, initialized using G-PAR, is presented. Finally, the ease of application of such a scheme to a multiple object tracking wrapper is demonstrated in brief.

1. INTRODUCTION

A single short-arc measurement from an SSA sensor like a radar or a telescope gives only partial-state information and is insufficient to initialize all the states of a Resident Space Object (RSO). In an ideal single object tracking scenario, Initial Orbit Determination (IOD) [8] schemes piece together multiple measurements from a single object, over time, and try to fit a state vector. This method assumes that the series of observations came from the same Resident Space Object (RSO). But in the Multiple Object Tracking (MOT) scenarios, with multiple observations in each frame, there would be combinatorial growth in the possible 'hard' observation-to-observation (obs-to-obs) associations[5]. It is also considerably easier to mathematically evaluate the likelihood of an observation associated with a cataloged object compared to keeping track and evaluating the likelihood of associating each observation (among many) in one pass to each observation (among many) in a second pass. In fact, for the overwhelming majority of multiple space-object tracking scenarios, a mathematically rigorous formulation for weighing one obs-to-obs association, between two sensor passes, versus another obs-to-obs association is impossible. This is because most objects appear the same to the sensor and even if identifying features like reflectivity and radar cross-sections could be measured making observation-to-observation associations using them remains ad-hoc in most cases.

A 'target' is defined as a RSO whose pdf is available in the space object catalog. The problem of finding correct obs-to-obs association can be avoided if it can be posed as a target-to-observation (sometimes also called track-to-observation, or track-to-obs) association problem. This can be done by initializing the pdf of the states of the RSO

Copyright © 2022 Advanced Maui Optical and Space Surveillance Technologies Conference (AMOS) – www.amostech.com

that generated the observation, forward propagating the said pdf using the dynamics equations, and calculating the measurement-likelihood of the measurements at the following passes. The initialization can be done using techniues like Constrained Admissible Region or Probabilistic Admissible Region algorithms.

The admissible region is the set of physically acceptable orbits that can be constrained even further if additional constraints on some orbital parameters like semi-major axis, eccentricity, etc, are present [11, 15, 16, 17]. This results in the constrained admissible region (CAR) [3, 4, 2]. If hard constraints are replaced, based on known statistics of the measurement process, with a probabilistic representation of the admissible region, it results in the probabilistic admissible region (PAR) [10]. PAR can be used for orbit initiation in Bayesian tracking [9].

Space Domain Awareness (SDA) telescopes usually take measurements of the Right Ascension and Declination of the RSOs. SDA telescopes can make these angles-only measurements very accurately, i.e. with very low values of standard deviation in measurement errors. This is especially true for observations of objects that are in, or higher than, Medium Earth Orbit. The PAR algorithm tries to map the postulated uncertainties in a few orbital parameters (a, e, i, Ω) and angles-only measurements of Right Ascension α, and Declination δ into the probability density function (pdf) of the states. This pdf can then be propagated and recursively updated using a Bayesian filter. It is shown that this initial pdf of states turns out to be multimodal, in which case it can be recursively updated by filters that handle multimodal pdf representation like the Particle Gaussian Mixture (PGM) filter.

The three contributions of this work are as follows:

- This paper presents a very simple, closed-form, geometric, solution that maps uncertainty in (a,e,i,Ω) and observations (α,δ) to the uncertainty in the states. This geometric solution to PAR, called G-PAR, is an improvement over the original PAR in ease of implementation, gives clear reasoning for the resulting multimodal pdf, and clearly explains why a sample could be inconsistent.
- Discusses the results of G-PAR based initialization for a RSO in MEO. It presents the results of integrating G-PAR with a Particle Gaussian Mixture (PGM) filter to recursively update the pdf of the RSO.
- Finally, a simple multiple object tracking problem with angles-only measurements is tackled using G-PAR for initialisation, PGM for underlying filtering, and a multi-object tracking filter, called R-FISST, as a wrapper to do hypotheses management.

2. TELESCOPE SENSOR MODEL

Modern SDA telescopes take measurements of the right ascension (α) and declination (δ) of the RSOs with respect to the sensor fixed, local East-North-Up (ENU) coordinate frame frame. For simulations presented in this paper, instead of this frame a coordinate frame whose axis are always parallel to the ECI reference frame, but is always centered on the sensor site, is being used on both the simulation (to generate measurements) and model (for measurement model that gets called by the filter). This has been done only for ease of implementation and reproduction of the results presented here and requires trivial modifications when using Local tangent plane coordinates like ENU. The measurement model can be written as follows:

$$\mathbf{y} = h(\mathbf{x}) + \nu \tag{1}$$

$$h(\mathbf{x}) = [\alpha, \delta]^T \tag{2}$$

where α, and δ are a function of the range vector $\boldsymbol{\rho}$, which can be found by:

$$\boldsymbol{\rho} = \mathbf{r} - \mathbf{q} \tag{3}$$

where $\mathbf{r}$ is the inertial position vector of the RSO and $\mathbf{q}$ is the inertial position vector of the sensor site.

$$\hat{\boldsymbol{\rho}} = [cos(\alpha)cos(\delta), \sin(\alpha)cos(\delta), sin(\delta)]^T \tag{4}$$

which gives:

$$\alpha = tan^{-1}\left(\frac{\hat{\boldsymbol{\rho}}(2)}{\hat{\boldsymbol{\rho}}(1)}\right) \tag{5}$$

Copyright © 2022 Advanced Maui Optical and Space Surveillance Technologies Conference (AMOS) – www.amostech.com

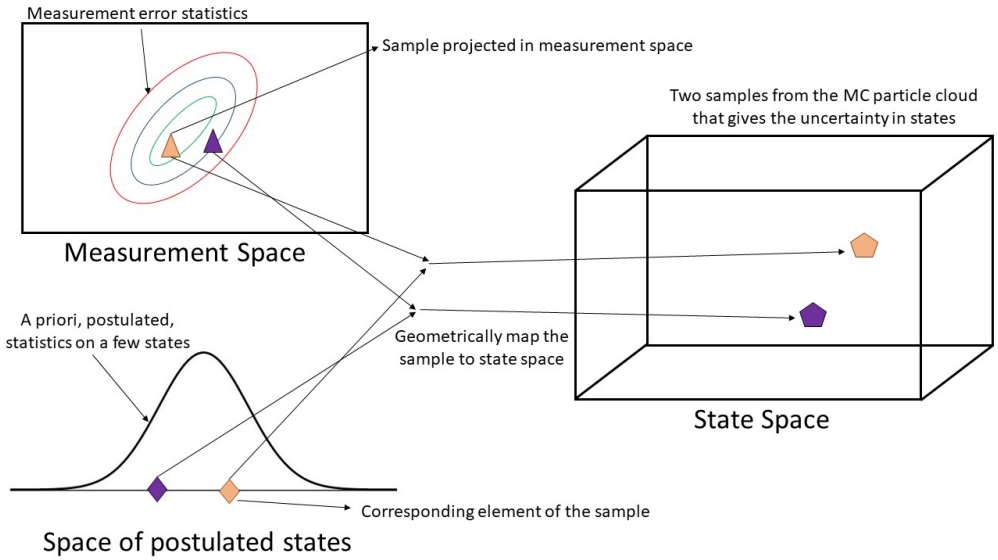

Fig. 1: Mapping samples from measurements and postulated states to the state space

$$\delta = tan^{-1}\left(\frac{\hat{\rho}(3)}{\hat{\rho}(1)\times(1/cos(\alpha))}\right) \tag{6}$$

Equation 6 is written in a somewhat unconventional form as a hint to use four quadrant inverse (atan2) when implementing these equations on a computer.

Detailed modelling of the complexities of a modern SDA telescopes, taking into account the slew rates, and field of view constraints, is beyond the scope of this work. It is acknowledged that the implementation of the algorithms being presented here on real data might have unforeseen limitations in tracking performance (but not on the initialization).

3. PROBABILISTIC ADMISSIBLE REGION (PAR)

The objective of PAR based algorithms is to get a probabilistic characterization of the uncertainty in the states given knowledge of the statistics of the measurement process and some statistics on the orbital parameters. The statistics on the orbital parameters could come from apriori knowledge, or be postulated based on the physics of the RSO population. In the angles-only case, the right ascension and declination (α,δ) observation and apriori knowledge of semi-major axis, a, eccentricity 2, inclination i, and right ascension of ascending node Ω are used to characterize the PAR.

The pdf of the measurements can be denoted by $p(\alpha,\delta)$. The distribution over (a,e,i,Ω), with slight abuse of notation, be denoted by $p(a,e,i,\Omega)$. For simplicity and without loss of generality, assume that these parameters are independent of each other, and from $p(\alpha,\delta)$. The joint distribution in $(a,e,i,\Omega,\alpha,\delta)$ can be written as:

$$p(a,e,i,\Omega,\alpha,\delta) = p(a)p(e)p(i)p(\Omega)p(\alpha,\delta) \tag{7}$$

4. GEOMETRIC SOLUTION TO PAR

A general template to get a geometrically map a single sample from the measurements and apriori-known states to state space for many different sensor modalities (angles-only telescope, angles-angle-rates telescope, or radar) is laid out as follows:

- Fix an orbital plane corresponding to the sample. In the telescope angles-only observation case, this can be done by using the sampled value of the Inclination and the sampled value of the Right ascension of ascending node.

Copyright © 2022 Advanced Maui Optical and Space Surveillance Technologies Conference (AMOS) – www.amostech.com

- Find the inertial position vector of the RSO corresponding to the sample. In the telescope angles-only observation case, this is done by finding the intersection of the line of sight vector (defined by the sampled values of right ascension and declination) with the orbital plane found in the previous step. If no such intersection exists for the sample then the elements of the sample are mutually-inconsistent.
- Find the elements of the velocity vector using the relevant equations or constraints. For the angles-only observation case, these are:
  - Velocity vector must lie on the orbital plane, and the unit angular momentum vector must be equal to the unit vector perpendicular to the orbital plane. The unit vector perpendicular to the orbital plane was found in the first step.
  - The velocity vector corresponding to the sample is related to the sampled values of semi-major axis and eccentricity. Even though these relations can be expressed algebraically using vis-viva equation (a and r are known) and eccentricity vector equation, it is easier to visualize and solve for velocity vector using geometry. The details of doing so will be covered in the following section.

4.1 Initialization: G-PAR MC particle cloud

Sample from : $p(a,e,i,\Omega,\alpha,\delta)$ to get $(a^j,e^j,i^j\Omega^j,\alpha^j,\delta^j)$.
Use i^j, and Ω^j to fix an orbital plane corresponding to the sample. This is done by defining the unit vector perpendicular to the orbital plane, $\hat{\mathbf{h}}^j$, using Equation 8.

$$\hat{\mathbf{h}}^j = [sin(i^j)sin(\Omega^j), -sin(i^j)cos(\Omega^j), cos(i^j)]^T \tag{8}$$

The inertial position vector corresponding to the sample can be written in terms of the inertial position vector of sensor site $\mathbf{q}$, and the relative position vector of the space object with respect to the sensor site $\boldsymbol{\rho}^j$. This is given by Equation 9.

$$\mathbf{r}^j = \mathbf{q}^j + \boldsymbol{\rho}^j \tag{9}$$

The relative position vector of the space object with respect to the sensor site $\boldsymbol{\rho}^j$ is not known but the unit relative position vector which is equal to the unit vector along the line of sight is known and is given by Equation 10.

$$\hat{\boldsymbol{\rho}}^j = [cos(\alpha^j)cos(\delta^j), sin(\alpha^j)cos(\delta^j), sin(\delta^j)]^T \tag{10}$$

Equation 9 can be re-written as:

$$\mathbf{r}^j = \mathbf{q}^j + k\hat{\boldsymbol{\rho}}^j \tag{11}$$

where k (a scalar) and $\mathbf{r}^j$ are unknowns. Use Equation 12 to find k.

$$\mathbf{r}^j \cdot \hat{\mathbf{h}}^j = (\mathbf{q}^j + k\hat{\boldsymbol{\rho}}^j) \cdot \hat{\mathbf{h}}^j = 0 \tag{12}$$

If k comes out to be negative, it means that the orbital plane is in the direction opposite to the line of sight, implying that the sampled values of (α^j,δ^j) and (i^j,Ω^j) are mutually inconsistent and therefore the sample is invalid. If k comes out to be positive, plug it into Equation 11 to get the the inertial position vector corresponding to the sample.

Check if the magnitude of the inertial position vector, r^j, is greater than the distance of perigee from the focus, i.e. center of the Earth, given by $a^j(1-e^j)$, and is lesser than the distance of the apogee from the focus, given by $a^j(1+e^j)$. If either of these conditions are violated then the sampled values of (a^j,e^j) are inconsistent with the sampled values of $(\alpha^j,\Delta^j,i^j,\Omega^j)$ and the sample should be discarded.

Let the elements of the unit angular momentum vector expressed in ECI reference frame be given by $\hat{\mathbf{h}} = [h_1,h_2,h_3]^T$. Let the three mutually perpendicular unit vectors that define the ECI, Cartesian coordinate frame be called $\hat{\mathbf{i}},\hat{\mathbf{j}},\hat{\mathbf{k}}$. Find

Copyright © 2022 Advanced Maui Optical and Space Surveillance Technologies Conference (AMOS) – www.amostech.com

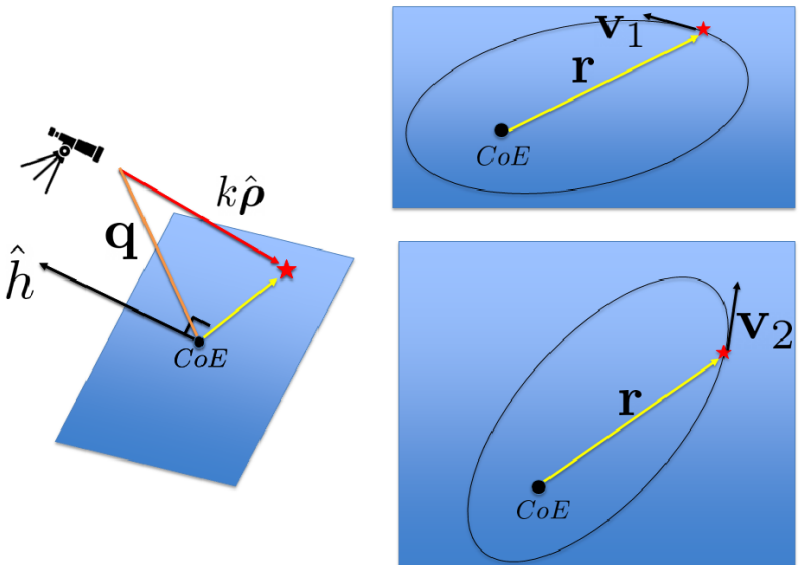

Fig. 2: Left: Visualizing the intersection of line of sight with the orbital plane for a particular sample, Right: The two possible orientations that the ellipse could take given that the object position, and the orbital plane is fixed.

the unit vector that points from the center of the earth to the ascending node, **b**, by taking the cross product of the vector perpendicular to the equatorial plane and the unit vector perpendicular to the orbital plane.

$$\mathbf{b} = (0\hat{i} + 0\hat{j} + 1\hat{k}) \times (h_1\hat{i} + h_2\hat{j} + h_3\hat{k}) = -h_2\hat{i} + h_1\hat{j} \tag{13}$$

The sum of the argument of perigee and true anomaly, $(\omega^j + \nu^j)$, corresponding to the sample can be found using the following relation:

$$\omega^j + \nu^j = cos^{-1}\left(\frac{\mathbf{b} \cdot \mathbf{r}^j}{\sqrt{\mathbf{b} \cdot \mathbf{b}}\sqrt{\mathbf{r}^j \cdot \mathbf{r}^j}}\right) \tag{14}$$

x that is the x-coordinate of the sample when looking at the orbital plane, the x-axis points towards the perigee, and the center of the earth is at one of the focii, is given as,

$$x = \frac{a^j - r^j}{e^j} \tag{15}$$

The relationship between x and the two possible values of true anomaly $\nu^{j,1}$ and $\nu^{j,2}$ are given by

$$\nu^{j,1} = cos^{-1}\left(\frac{x - a^j e^j}{r^j}\right) \tag{16}$$

$$\nu^{j,2} = -cos^{-1}\left(\frac{x - a^j e^j}{r^j}\right) \tag{17}$$

Plug these into Equation 14 to get the two corresponding values of $\omega^{j,1}$ and $\omega^{j,2}$.

A sample $(a^j, e^j, i^j, \Omega^j, \alpha^j, \delta^j)$ was mapped into two sets of Keplerian orbital elements $(a^j, e^j, i^j, \Omega^j, \omega^{j,1}, \nu^{j,1})$ and $(a^j, e^j, i^j, \Omega^j, \omega^{j,2}, \nu^{j,2})$. Transform both these from Keplerian orbital elements to ECI Cartesian-coordinate, position-velocity elements to get two corresponding samples in position-velocity space. Repeat this mapping process for an ensemble of samples drawn from $p(a, e, i, \Omega, \alpha, \delta)$ to get the G-PAR particle cloud that captures the uncertainty in the position and velocity given measurements, measurement error statistics, and postulates statistics on some states.

Figure 3 shows the resulting G-PAR particle cloud for a MEO object with ground truth given by the following:

$$[a, e, i, \Omega, \omega, \nu]^T = [27500 \text{ km}, .05, 55^\circ, -13.24^\circ, -60^\circ, 120^\circ] \tag{18}$$

Copyright © 2022 Advanced Maui Optical and Space Surveillance Technologies Conference (AMOS) – www.amostech.com

The following postulated statistics were used to initialize the G-PAR particle cloud:

$$a \sim \mathscr{U}(25{,}000km, 30{,}000km) \tag{19}$$

$$e \sim \mathscr{U}(0, 0.1) \tag{20}$$

$$i \sim \mathscr{U}(50^\circ, 65^\circ), \tag{21}$$

$$\Omega \sim \mathscr{U}(-23.24^\circ, 0^\circ), \tag{22}$$

where $\mathscr{U}(a,b)$ denotes a uniform distribution between a and b.

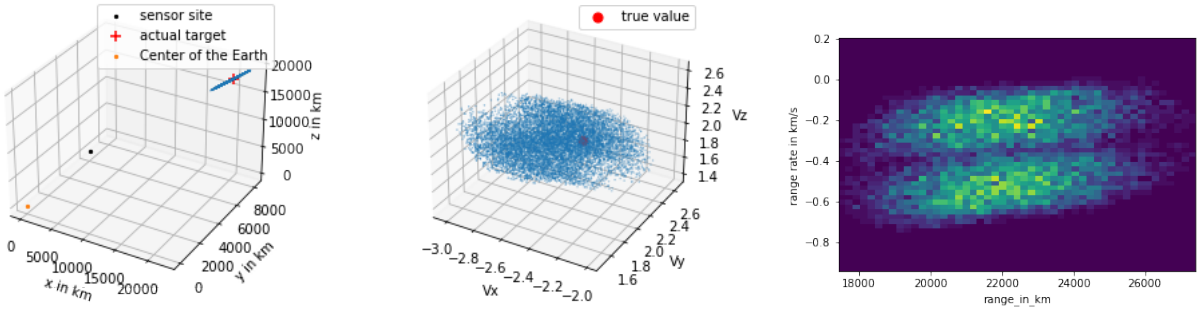

Fig. 3: Left: PAR Particle cloud in x-y-z space, Middle: PAR Particle cloud in ẋ-ẏ-ż space, Right: Density of the PAR particles projected into $\rho - \dot{\rho}$ space

The rightmost sub-figure in Figure 3 shows the density of the particles in the range vs range-rate space. It can be clearly seen that there are two distinct lobes one with positive range rate and another with negative range rate consistent with how the two solutions for each sample that were expected. Similar multi modal behavior can be observed in the middle sub-figure where there are two distinct lobes in the velocity particle cloud. The leftmost sub-figure in Figure 3 shows the density of the particles in the position space and as expected the particle cloud is long and thing, basically stretching along the line of sight.

5. RECURSIVE UPDATE

Particle Gaussian Filter (PGM)[13, 14] employs an ensemble of possible state realizations for the propagation of the state probability density. A Gaussian mixture model (GMM) of the propagated uncertainty is then recovered by clustering the ensemble. Subsequently, the posterior density is obtained through a Kalman measurement update of the mixture modes.

Algorithm 1 Particle Gaussian Mixture Filter

1: Given $\pi_0(x_0) = \sum_{i=0}^{M(0)} w_i(0)\mathscr{G}_i(x_0; \mu_i(0), P_i(0))$, transition density kernel $p_n(x|x'), n = 1$
2: Sample N_p particles $X^{(i)}$ from π_{n-1} and the transition kernel $p_n(x|x')$ as follows: Sample $X^{(i)'}$ from $\pi_{n-1}(.)$, Sample $X^{(i)}$ from $p(.|X^{(i)'})$.
3: Use a clustering algorithm $\mathscr{C}$ to cluster the set of particles $X^{(i)}$ into $M^-(n)$ Gaussian clusters with weights, mean and covariance given by $\{w_i^-(n), \mu_i^-(n), P_i^-(n)\}$
4: Update the mixture weights and mixture means and covariance to $\{w_i(n), \mu_i(n), P_i(n)\}$, given the observation z_n, utilizing the Kalman update (Equations 23,24)
5: $n = n+1$, go to Step 2.

Consider the measurement update, given that the prior component is Gaussian, and if the update is approximated using the Kalman/linear minimum mean squared error (LMMSE) update, we have:

$$\mu_i(n) = \mu_i^-(n) + P_{i,zx}^T(n) P_{i,zz}^{-1}(n)(z_n - E_i[h(X)]), \tag{23}$$

Copyright © 2022 Advanced Maui Optical and Space Surveillance Technologies Conference (AMOS) – www.amostech.com

$$P_i(n) = P_i^-(n) - P_{i,zx}^T(n) P_{i,zz}^{-1}(n) P_{i,zx}(n), \tag{24}$$

where

$$P_{i,zx}(n) = E_i\Big[\big(h(X) - E_i(h(X))\big)\big(X - E_i(X)\big)^T\Big], \tag{25}$$

$$P_{i,zz}(n) = E_i\Big[\big(h(X) - E_i(h(X))\big)\big(h(X) - E_i(h(X))\big)^T\Big], \tag{26}$$

5.1 Dynamics

Simple two body dynamics is considered on the simulation as well as the model side. The elements of the inertial position, **r**, and velocity, **v**, vectors of the RSO comprise the vector of the states, **x**, of the RSO.

$$\mathbf{x} = \begin{bmatrix} \mathbf{r} \\ \mathbf{v} \end{bmatrix}$$
$$\dot{\mathbf{r}} = \mathbf{v}$$

Where the equation of motion is:

$$\ddot{\mathbf{r}} = -\frac{GMm}{r^3}\mathbf{r} \tag{27}$$

Although higher order gravitational terms (J2 and onwards), or other effects like solar radiation pressure that cause perturbations have not been considered, it is straightforward to include them in the propagation equations of each particle. Because of assumption about perfect modelling of the dynamics, no process noise term is included in the filter. Note, that these simplifying assumptions, about dynamics and process noise, were made to keep the focus on G-PAR, and are not necessary for G-PAR or the PGM filter implementation.

5.2 Measurements

It was assumed that the SDA telescope generates an angles measurement every 45 seconds. The measurement error covariance matrix was given by:

$$R = \begin{bmatrix} (2 \text{ arcsec})^2 & 0 \\ 0 & (2 \text{ arcsec})^2 \end{bmatrix} \tag{28}$$

which among other things, tells that the standard deviation of the errors made in angle measurements (α, δ) were only 2 arcseconds each.

A six component Gaussian Mixture Model (GMM) was used in the update step from timestep 1 through 10. Subsequently, a single component Gaussian representation was used. Figures 4, 5, and 6 show the particle cloud after measurement update at different time steps. Note that the object always remain well tracked.

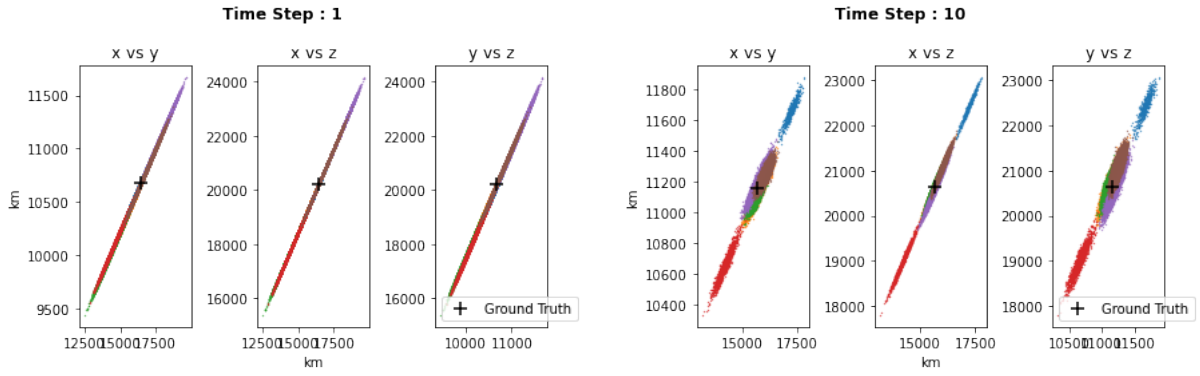

Fig. 4: Left: PAR Particle cloud in x-y, x-z, and y-z space after measurement update at time step 1, Right: PAR Particle cloud in x-y, x-z, and y-z space after measurement update at time step 10

Copyright © 2022 Advanced Maui Optical and Space Surveillance Technologies Conference (AMOS) – www.amostech.com

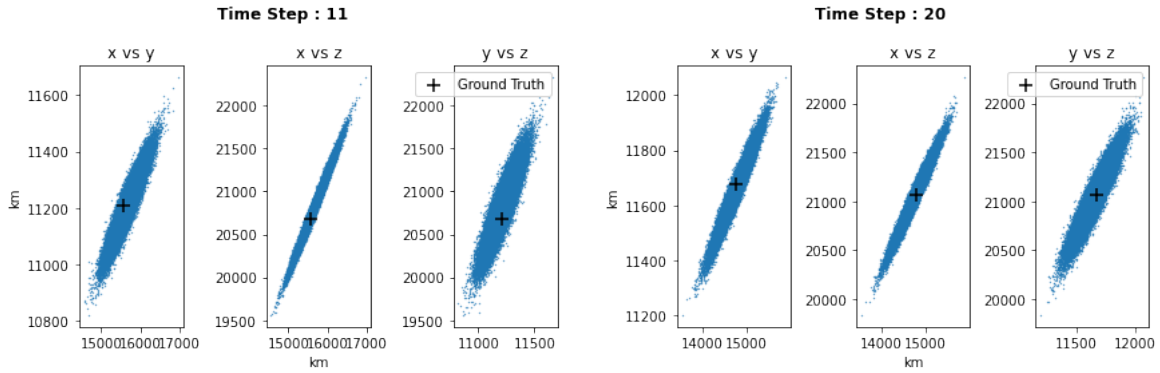

Fig. 5: Left: PAR Particle cloud in x-y, x-z, and y-z space after measurement update at time step 11, Right: PAR Particle cloud in x-y, x-z, and y-z space after measurement update at time step 20

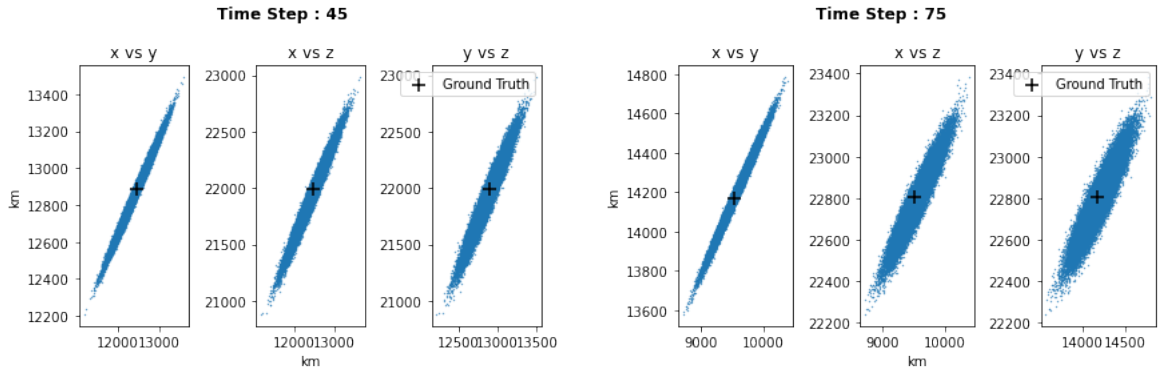

Fig. 6: Left: PAR Particle cloud in x-y, x-z, and y-z space after measurement update at time step 45, Right: PAR Particle cloud in x-y, x-z, and y-z space after measurement update at time step 75

6. MULTI OBJECT TRACKING

A Multi target tracking simulation with angles-only observations from a ten object debris cloud, but with no false-alarm/clutter, in MEO was created. All the objects had the same a, e, i, Ω, ω but different ν The ground truth for the objects was given by:

$$[a, e, i, \Omega, \omega, \nu]^T = [27500 \text{ km}, .05, 55^\circ, -13.24^\circ, -60^\circ] \tag{29}$$

$$[\nu_1, ..., \nu_{10}] = [116^\circ, 117^\circ, 117.2^\circ, 118^\circ, 119.8^\circ, 120^\circ, 120.1^\circ, 120.5^\circ, 121^\circ, 122.1^\circ] \tag{30}$$

A hypotheses management wrapper called R-FISST II [12, 6, 7] armed with G-PAR for track initialization, and an underlying PGM filter for recursive update, with six component GMM for first ten time steps post initialization and a single component, simple Gaussian in the subsequent time steps, was used. All other relevant parameters (measurement cadence, ...) and information (measurement model, measurement error statistics, ...)remains unchanged from the single obect tracking example. Figures 7, 8, 9, and 10 show the propagated states of the pdfs of the ten objects at different time steps. Note that Figure 9 shows two objects that were 're-initialized' (hence the multi modal pdf). This can happen if the R-FISST II's inbuilt thresholds for minimum allowed likelihood are violated. In such cases R-FISST II can automatically 'kill' an object with a very inflated (due to long propagation without update) pdf and seed a new object in it's place. It can be seen that all objects remain reasonably well tracked.

Copyright © 2022 Advanced Maui Optical and Space Surveillance Technologies Conference (AMOS) – www.amostech.com

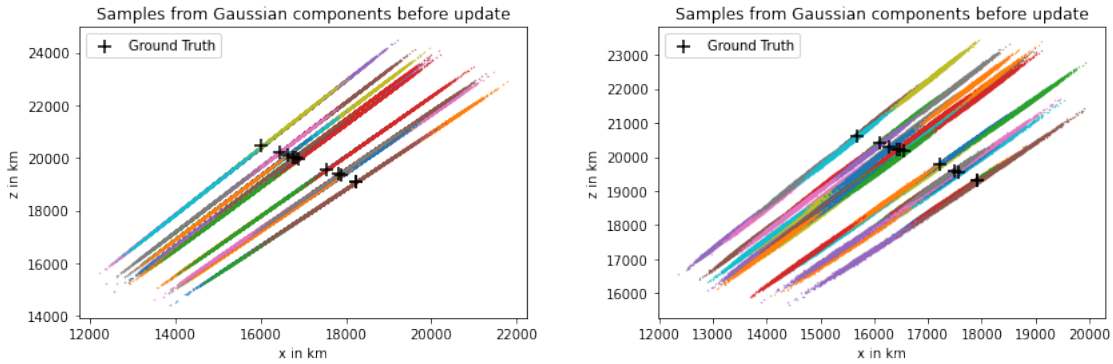

Fig. 7: Left: Propagated particle clouds in x-z space before measurement update at time step 1, Right: Propagated particle clouds in x-z space before measurement update at time step 5

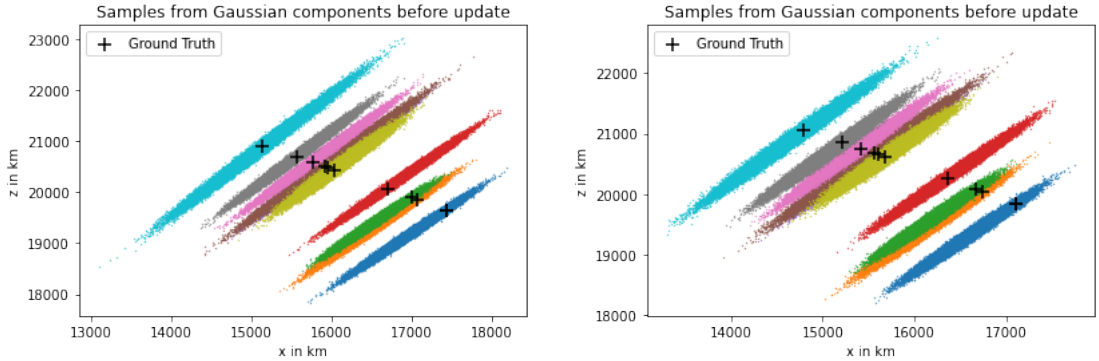

Fig. 8: Left: Propagated particle clouds in x-z space before measurement update at time step 11, Right: Propagated particle clouds in x-z space before measurement update at time step 15

7. CONCLUSION

A geometric solution to probabilistic admissible region was presented. The uncertainty in (α, δ) measurements and apriori knowledge about (a, e, i, Ω), were mapped into uncertainty in the states. The MC particle cloud obtained by G-PAR was then used to initialize a PGM filter with a single Gaussian component. The filter was used to recursively update the pdf using successive observations. It was shown that object remains well tracked.

G-PAR algorithms are very well suited in a large number of practical scenarios like multiple object tracking in orbit collision or Anti-Satellite weapon testing and uncooperative launches and swarm deployments. The assumptions being made regarding apriori knowledge about the right ascension of ascending node and semi-major axis hold well in such cases. There is also the added advantage of automating the association problem in such multi object tracking cases[12, 1].

Future work would focus on improving the clustering schemes used in PGM, coming up with analog of showcasing tracking performance by plotting errors in estimated states vs ground truth with +/- 3-sigma bounds for multi-modal PGM, and implementing more realistic multi-target tracking simulations.

8. ACKNOWLEDGEMENTS

The authors are thankful to Dr. Erik Blasch, AFOSR and AFWERX for providing generous funding to support this research work via contract no. FA9550-21-P-0008.

Copyright © 2022 Advanced Maui Optical and Space Surveillance Technologies Conference (AMOS) – www.amostech.com

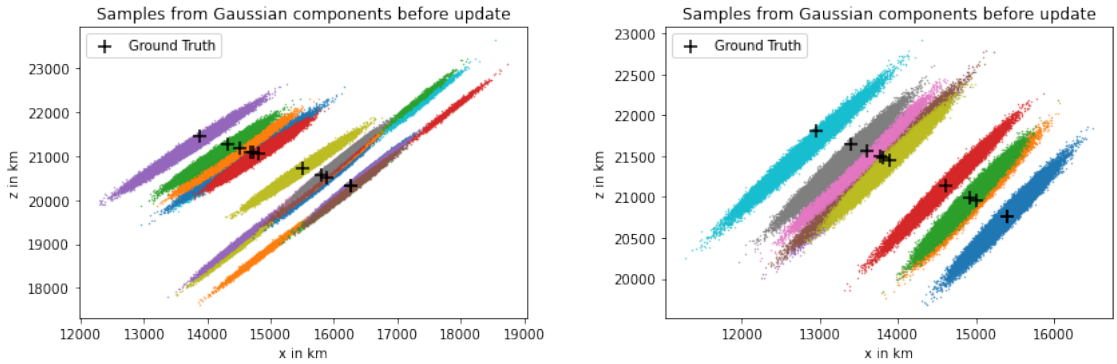

Fig. 9: Left: Propagated particle clouds in x-z space before measurement update at time step 25, Right: Propagated particle clouds in x-z space before measurement update at time step 35

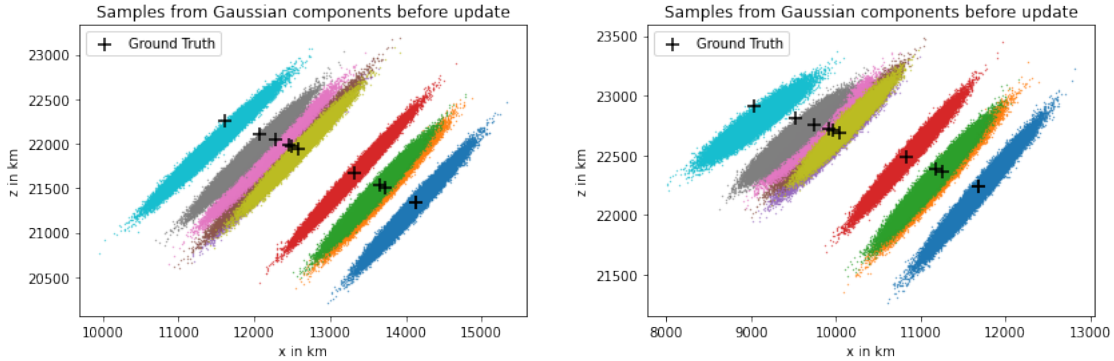

Fig. 10: Left: Propagated particle clouds in x-z space before measurement update at time step 50, Right: Propagated particle clouds in x-z space before measurement update at time step 75

9. REFERENCES

[1] S. Chakravorty, W. R. Faber, I. I. Hussein, and U. R. Mishra. A belief space perspective of rfs based multi-target tracking and its relationship to mht. *ArXiv e-prints*, 2020.

[2] Kyle J. DeMars and Moriba K. Jah. Evaluation of the information content of observations with application to sensor management for orbit determination. *Advances in the Astronautical Sciences*, 142, 2011. (Proceedings of the AAS/AIAA Astrodynamics Specialist Conference, Girdwood, AK, July 31–August 4 2011, Paper AAS 11-606).

[3] Kyle J. DeMars and Moriba K. Jah. Initial orbit determination via gaussian mixture approximation of the admissible region. *Advances in the Astronautical Sciences*, 143, 2012. (Proceedings of the 22nd AAS/AIAA Space Flight Mechanics Meeting, Charleston, SC, January 29–February 2 2012, Paper AAS 12-260).

[4] Kyle J. DeMars and Moriba K. Jah. Probabilistic initial orbit determination using gaussian mixture models. *Journal of Guidance, Control, and Dynamics*, 36(5):1324–1335, September–October 2013.

[5] W. Faber, S. Chakravorty, and I. Hussein. Multi-object tracking with multiple birth, death, and spawn scenarios using a randomized hypothesis generation technique (RFISST). In *Proceedings of the 19th International Conference on Information Fusion*, pages 154–161, Darmstadt, Germany, 2016. IEEE.

[6] W.R. Faber, U.R. Mishra, S. Chakravorty, and I. Hussein. Mcmc sampling and clustering methods for a randomized finite set statistics technique (rfisst-ii). 2020. (Proceedings of the AAS/AIAA Astrodynamics Specialist Conference, Lake Tahoe, CA, Paper AAS 20-776).

[7] W.R. Faber, U.R. Mishra, S. Chakravorty, and I. Hussein. Application of a randomized-finite set statistics technique (r-fisst) to space situational awareness. *Journal of Astronautical Sciences*, 2022.

[8] Robert H. Gooding. A new procedure for the solution of the classical problem of minimal orbit determination

Copyright © 2022 Advanced Maui Optical and Space Surveillance Technologies Conference (AMOS) – www.amostech.com

from three lines of sight. *Celestial Mechanics and Dynamical Astronomy*, 66(4):387–423, 1997.

[9] Islam I. Hussein, Christopher W. T. Roscoe, Paul W. Schumacher, Jr., and Matthew P. Wilkins. Probabilistic admissible region for short-arc angles-only observation. In *Proceedings of the Advanced Maui Optical and Space Surveillance Technologies Conference*, Wailea, HI, September 9–12 2014.

[10] Islam I. Hussein, Christopher W. T. Roscoe, Matthew P. Wilkins, and Paul W. Schumacher, Jr. Probabilistic admissibility in angles-only initial orbit determination. In *Proceedings of the 24th International Symposium on Space Flight Dynamics*, Laurel, MD, May 5–9 2014.

[11] T. Kelecy, M. Shoemaker, and M. Jah. Application of the constrained admissible region multiple hypothesis filter to initial orbit determination of a break-up. *Proceedings of the 6th European Conference on Space Debris Darmstadt, Germnay*, 08/2013.

[12] U.R. Mishra, W.R. Faber, S. Chakravorty, and I. Hussein. Applications of a mcmc sampling and clustering methods based randomized-finite set statistics technique (r-fisst ii). 2021. (31st AAS/AIAA Space Flight Mechanics Meeting).

[13] D. Raihan and S. Chakravorty. Particle gaussian mixture filterss. Technical Report arXiv:1603.04510, arXiv, 2016.

[14] D. Raihan and S. Chakravorty. Particle gaussian mixture (PGM) filters. In *Proceedings of the 19th International Conference on Information Fusion*, pages 1369–1376, Piscataway, NJ, 2016. IEEE.

[15] Christopher W. T. Roscoe, Islam I. Hussein, Matthew P. Wilkins, and Paul W. Schumacher, Jr. The probabilistic admissible region with additional constraints. *Advances in the Astronautical Sciences*, 156:117–130, 2015. (Proceedings of the AAS/AIAA Astrodynamics Specialist Conference, Vail, CO, August 9–13 2015, Paper AAS 15-577).

[16] Christopher W. T. Roscoe, Paul W. Schumacher, Jr., and Matthew P. Wilkins. Parallel track initiation for optical space surveillance using range and range-rate bounds. *Advances in the Astronautical Sciences*, 150:989–1008, 2014. (Proceedings of the AAS/AIAA Astrodynamics Specialist Conference, Hilton Head, SC, August 11–15 2013, Paper AAS 13-767).

[17] Christopher W. T. Roscoe, Matthew P. Wilkins, Islam I. Hussein, and Paul W. Schumacher, Jr. Uncertain angles-only track initiation for SSA using different iod methods. *Advances in the Astronautical Sciences*, 158, 2016. (Proceedings of the 26th AAS/AIAA Space Flight Mechanics Meeting, Napa, CA, February 14–18 2016, Paper AAS 16-207).

Copyright © 2022 Advanced Maui Optical and Space Surveillance Technologies Conference (AMOS) – www.amostech.com